Water Column Current Profile Aided Localisation for Autonomous Underwater Vehicles

Lashika Medagoda, Mike V. Jakuba, Oscar Pizarro, Stefan B. Williams
Australian Centre for Field Robotics
University of Sydney, Sydney NSW 2006 Australia
{l.medagoda,m.jakuba,o.pizarro,stefanw}@acfr.usyd.edu.au

***Abstract*—Survey class Autonomous Underwater Vehicles (AUVs) rely on Doppler Velocity Logs (DVL) for precise navigation near the seafloor. In cases where the seafloor depth is greater than the DVL bottom lock range, transiting from the surface, where GPS is available, to the seafloor presents a localisation problem since both GPS and DVL are unavailable in the mid-water column. This paper proposes an alternative approach to navigation in the mid-water column that exploits the fact that current profiles of water columns are stable over time. With reobservation of these currents with the ADCP (Acoustic Doppler Current Profiler) mode of the DVL during descent, along with sensor fusion of other low cost sensors, position error growth can be constrained to near the initial velocity uncertainty of the vehicle at the sea surface during the dive, and following DVL bottom lock, the entire velocity history is constrained to an error similar to the DVL velocity uncertainty. Simulation results show performance with sensor fusion of a low cost IMU and DVL bottom lock at the sea floor can achieve 20 cm per minute (2 σ) position error growth. Results with real data from an Autonomous Benthic Explorer (ABE) dive show that this method is applicable and a promising approach to navigation for untended deepwater autonomous vehicle operations.**

I. Introduction

Autonomous Underwater Vehicles (AUVs) have found application in general underwater exploration and monitoring. This includes high-resolution, georeferenced optical/acoustic oceanfloor mapping, along with providing water column information such as currents, temperature and salinity. An advantage of AUVs over other methods of ocean observation is the autonomy and decoupling from the sea surface that a self-contained vehicle provides.

Georeferencing is important for AUVs to place their mission in the correct position in a global reference frame, for the purpose of path planning for mission requirements, registration with independently navigated information, or revisiting a previous mission. For shallow waters, low frequency, high power Doppler Velocity Log (DVL) can be in continuous use for depths less than 200m. The DVL sensor provides measurements of the seafloor relative velocity of the AUV. By combining this information with an appropriate heading reference, the observations can be placed in the global reference frame and integrated to facilitate underwater dead reckoning. Accuracies of O(22m) per hour (2σ) in position error growth is attainable during diving, and coupled with a navigation grade (>\$100K) Inertial Measurement Unit (IMU), O(8m) per hour error growth (2σ) is possible [11]. IMUs provide body-relative accelerations and rotation rates to provide constraints for position, velocity and attitude. Simultaneous Localisation and Mapping (SLAM) methods allow further navigation improvements [18].

In cases where the seafloor depth is greater than the DVL bottom lock range, transiting from the surface, where GPS is available, to the seafloor presents a localisation problem since both GPS and DVL are unavailable in the mid-water column. Traditional solutions during this descent include range-limited Long Base Line (LBL) acoustic networks which require additional ship time to deploy and survey, along with methods requiring tending such as ship based Ultra Short Base Line (USBL). USBL also suffers from multipath returns and the sound speed profile through the water column needs to be accurately known. These acoustic methods typically give O(10m) accuracy [7] [9].

On board sensors to aid localisation in the mid-water column, which do not rely on external acoustics such as LBL or USBL, include IMUs and DVL in water track mode. The DVL in water track mode provides a measurement of the velocity of the AUV relative to a user-programmable water sampling volume that extends away from the instrument. A navigation grade IMU coupled with a vehicle model and DVL water track mode estimates of currents can achieve O(2m) per minute (2σ) position error growth [5].

For a typical dive rate of 20 metres per minute, a 1 kilometre dive will take 50 minutes. Thus, without relying on externally deployed acoustic methods such as USBL and LBL, relying on the state-of-the-art IMU/Vehicle model/DVL water track will give O(100m) (2σ) accuracy. Thus, missions requiring revisit capabilities in depths beyond a few hundred metres must invest in the greater effort of external acoustic methods such as LBL. This is the typical mode of operation for vehicles such as ABE when searching for hydrothermal vents [6]. This requirement for establishing LBL infrastructure motivates the need for a higher accuracy solution using only onboard instruments to give AUVs true autonomy.

This paper proposes an alternative approach to navigation in the mid-water column that exploits the fact that current profiles of water columns are stable over time. With reobservation of these currents with the ADCP (Acoustic Doppler Current Profiler) mode of the DVL during descent, along with sensor fusion of other low cost sensors, position error growth can be constrained to near the initial velocity uncertainty of the vehicle at the sea surface during the dive, and following DVL bottom lock, the entire velocity history is constrained to an

978-1-4244-5222-4/10/\$26.00 ©2010 IEEE

error similar to the DVL velocity uncertainty.

The remainder of this paper is organised as follows. Section II introduces the ADCP sensor and its operation, along with previous related work, and an explanation of the proposed method and theory. Section III presents results to validate the proposed method. Section IV concludes with discussion of future direction and the implications of this work.

II. ADCP AIDING

An alternative to using the bulk water volume relative velocity from the DVL water track mode [5] is to instead use the Acoustic Doppler Current Profiler (ADCP) mode to provide finer depth resolution current estimation. This opens the possibility of improved vehicle motion estimates, given the observation of fine scale current structure.

A. ADCP sensor operation

The ADCP operates by sending out an acoustic pulse, and relying on scatterers, such as plankton, to reflect back the pulse. Using the Doppler effect, the velocity of the scatterers relative to the instrument can be determined in the radial direction. Since it is assumed that the scatterers move with the water currents, the ADCP is measuring the radial velocity of the water column. By gating the returned signal with time, currents at different ranges from the ADCP sensor can be measured, segmenting the observation into measurement cells. By using 4 differently aligned sensors and assuming horizontally homogeneous currents, the 3D velocity of the current can be determined. The fourth sensor provides redundancy in the estimation of the current profile velocities [4]. Echo intensity can also be used to check if there are anomalies corrupting the returns, such as schools of fish [12]. The result is a current estimate with accuracies typically about 10 mm/s (2σ) observing 2 m/s currents[1].

B. Related work

Previous work regarding the use of ADCP sensors falls within either the oceanographic community, or the underwater localisation field.

The focus within the oceanographic community is on estimating water current profiles, such as applying least squares methods to fuse ADCP and DVL bottom lock information [17]. Accounting for ADCP sensor biases [4] and sensor uncertainties are not tackled, as the effect on the overall current profile is minimal, although there are implications in the velocity estimates of the ADCP sensor during the descent, which is important for localisation as the velocity uncertainty relates to the position error growth rate.

In the underwater localisation field, currents are typically treated as a single time varying parameter [10] using observations from the DVL water track mode. This approach does not take advantage of the finer structure of the currents nor exploit their stability over time. Horizontally looking ADCPs have been employed to map current fields in [3], but have not been used to aid with localisation.

[1]Sourced from email from RD Instruments providing standard deviation of the instrument

C. ADCP estimation and navigation aiding method

We assume that initially, the AUV is assumed to have position and velocity estimates in the navigation frame at the sea surface from GPS. With the ADCP sensor, body-relative water current bin velocities below the vehicle are observed with each ADCP measurement cell. These observations can be used to estimate the full current profiles in the navigation frame using the estimated vehicle velocity at the surface. This is illustrated in Figure 1(a).

After another ADCP measurement is made, the vehicle reobserves the same current bins. Given the estimated water current velocity of the reobserved current bin and the body-relative velocity of these current bins from the ADCP a filter can be used to simultaneously update the estimate of the vehicle velocity and current profile velocities.. This relies on the assumption that the water current velocity in this bin remains constant, which is realistic over a reobservation period of minutes. This is shown in Figure 1(b).

New current bins can also now be estimated as the vehicle changes depth as shown in Figure 1(c). The result is an estimate of the vehicle motion and a water column current profile. When the vehicle is within DVL range of the seafloor, this body-relative velocity constraint on the vehicle is also incorporated into the filter.

1) Information filter with current profiling: A sparse extended information filter (SEIF) estimates the states of the vehicle given the various vehicle sensors [14]. This simply accommodates the water current states and allows relinearisation or smoothing if required. The SEIF maintains the correlations between states. Vehicle pose states (position, velocity and attitude), ADCP bias states and water current velocity states are stored in a state vector in the form

$$\hat{\mathbf{x}}^+(t_k) = \begin{bmatrix} \hat{\mathbf{x}}^+_{p_1}(t_k) \\ \vdots \\ \hat{\mathbf{x}}^+_{p_{n_p}}(t_k) \\ \hat{\mathbf{x}}^+_{b_{c,1}}(t_k) \\ \vdots \\ \hat{\mathbf{x}}^+_{b_{c,n_b}}(t_k) \\ \hat{\mathbf{x}}^+_{v_{c,n}}(t_k) \\ \vdots \\ \hat{\mathbf{x}}^+_{v_{c,n_v}}(t_k) \end{bmatrix} = \begin{bmatrix} \hat{\mathbf{x}}^+_{p}(t_k) \\ \hat{\mathbf{x}}^+_{b_c}(t_k) \\ \hat{\mathbf{x}}^+_{v_c}(t_k) \end{bmatrix} \tag{1}$$

where $\hat{\mathbf{x}}^+_p(t_k) = \begin{bmatrix} \hat{\mathbf{x}}^{+\mathsf{T}}_{p_1}(t_k), ..., \hat{\mathbf{x}}^{+\mathsf{T}}_{p_{n_p}}(t_k) \end{bmatrix}^\mathsf{T}$ is a vector of past and present pose states where n_p is the number of vehicle pose states, $\hat{\mathbf{x}}^+_{b_c}(t_k) = \begin{bmatrix} \hat{\mathbf{x}}^{+\mathsf{T}}_{b_{c,1}}(t_k), ..., \hat{\mathbf{x}}^{+\mathsf{T}}_{b_{c,n_b}}(t_k) \end{bmatrix}^\mathsf{T}$ is a vector of past and present ADCP bias states where n_b is the number of ADCP bias states and $\hat{\mathbf{x}}^+_{v_c}(t_k) = \begin{bmatrix} \hat{\mathbf{x}}^{+\mathsf{T}}_{v_{c,1}}(t_k), ..., \hat{\mathbf{x}}^{+\mathsf{T}}_{v_{c,n_v}}(t_k) \end{bmatrix}^\mathsf{T}$ is a vector of past and present ADCP water current velocity states where n_v is the number of water current velocity states. The covariance between the pose states and the water current states are in the form

$$\hat{\mathbf{P}}^+(t_k) = \begin{bmatrix} \hat{\mathbf{P}}^+_{pp}(t_k) & \hat{\mathbf{P}}^+_{pb_c}(t_k) & \hat{\mathbf{P}}^+_{pv_c}(t_k) \\ \hat{\mathbf{P}}^{+\mathsf{T}}_{pb_c}(t_k) & \hat{\mathbf{P}}^+_{b_cb_c}(t_k) & \hat{\mathbf{P}}^+_{b_cv_c}(t_k) \\ \hat{\mathbf{P}}^{+\mathsf{T}}_{pv_c}(t_k) & \hat{\mathbf{P}}^{+\mathsf{T}}_{b_cb_c}(t_k) & \hat{\mathbf{P}}^+_{v_cv_c}(t_k) \end{bmatrix} \tag{2}$$

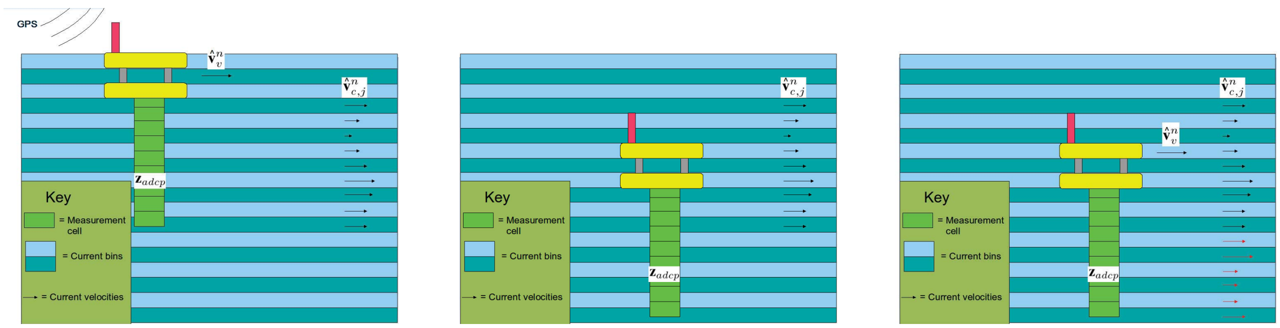

(a) (b) (c)

Fig. 1. ADCP aiding method sequence (a) Initial GPS position and velocity are known, and water velocities can be deduced. (b) The AUV moves, and reobserves the same current bins.(c) The AUV velocity in the world frame can be deduced, along with new current bins shown in red.

In the information form, the filter maintains the matrix $\mathbf{Y}$, which is the inverse of the covariance matrix

$$\hat{\mathbf{Y}}^{+}(t_k) = [\hat{\mathbf{P}}^{+}(t_k)]^{-1} \tag{3}$$

and the information vector $\mathbf{y}$, which is related to the state estimate by

$$\hat{\mathbf{y}}^{+}(t_k) = \hat{\mathbf{Y}}^{+}(t_k)\hat{\mathbf{x}}^{+}(t_k) \tag{4}$$

The information vector has the form

$$\hat{\mathbf{y}}^{+}(t_k) = \begin{bmatrix} \hat{\mathbf{y}}_p^{+}(t_k) \\ \hat{\mathbf{y}}_{b_c}^{+}(t_k) \\ \hat{\mathbf{y}}_{v_c}^{+}(t_k) \end{bmatrix} \tag{5}$$

and the information matrix has the form

$$\hat{\mathbf{Y}}^{+}(t_k) = \begin{bmatrix} \hat{\mathbf{Y}}_{pp}^{+}(t_k) & \hat{\mathbf{Y}}_{pb_c}^{+}(t_k) & \hat{\mathbf{Y}}_{pv_c}^{+}(t_k) \\ \hat{\mathbf{Y}}_{pb_c}^{+\mathsf{T}}(t_k) & \hat{\mathbf{Y}}_{b_c b_c}^{+}(t_k) & \hat{\mathbf{Y}}_{b_c v_c}^{+}(t_k) \\ \hat{\mathbf{Y}}_{pv_c}^{+\mathsf{T}}(t_k) & \hat{\mathbf{Y}}_{b_c b_c}^{+\mathsf{T}}(t_k) & \hat{\mathbf{Y}}_{v_c v_c}^{+}(t_k) \end{bmatrix} \tag{6}$$

Observations, which include ADCP measurements, are assumed to be made according to

$$\mathbf{z}(t_k) = \mathbf{h}[\mathbf{x}(t_k)] + \nu(t_k) \tag{7}$$

in which $\mathbf{z}(t_k)$ is an observation vector, $\mathbf{h}[\mathbf{x}(t_k)]$ is the sensor model relating states to observations, and $\nu(t_k)$ is a vector of observation errors with covariance $\mathbf{R}(t_k)$ New information from sensor measurements are incorporated into the information vector and matrix

$$\hat{\mathbf{y}}^{+}(t_k) = \hat{\mathbf{y}}^{-}(t_k) + \mathbf{i}(t_k) \tag{8}$$

$$\hat{\mathbf{Y}}^{+}(t_k) = \hat{\mathbf{Y}}^{-}(t_k) + \mathbf{I}(t_k) \tag{9}$$

in which

$$\begin{aligned} \mathbf{i}(t_k) \quad = \quad & \nabla_x^{\mathsf{T}}\mathbf{h}(t_k)\mathbf{R}^{-1}(t_k)(\mathbf{z}(t_k)\ldots \\ & -\mathbf{h}[\hat{\mathbf{x}}^{-}(t_k)] + \nabla_x\mathbf{h}(t_k)\hat{\mathbf{x}}^{-}(t_k)) \end{aligned} \tag{10}$$

$$\mathbf{I}(t_k) = \nabla_x^{\mathsf{T}}\mathbf{h}(t_k)\mathbf{R}^{-1}(t_k)\nabla_x\mathbf{h}(t_k) \tag{11}$$

where $\hat{\mathbf{x}}^{-}(t_k)$ is the *a priori* state estimate and $\nabla_x\mathbf{h}(t_k)$ is the Jacobian of the observation with respect to the state. Poses and current states which are no longer observed in the filter can be marginalised out to reduce the computational requirements of the filter, although this results in those past states being lost in the estimation. By keeping the entire state history the filter behaviour can be better analysed.

2) ADCP observation equation: The observation function for each ADCP measurement is

$$\mathbf{z}_{adcp,i} = \mathbf{C}_n^b(-\mathbf{v}_v^n + \sum \mathbf{W}_j\mathbf{v}_{c,j}^n) + \mathbf{b}_{c,i} + \nu_{adcp} \tag{12}$$

where:

- $\mathbf{z}_{adcp,i}$ = ADCP measured current vector in the ith measurement cell
- $\mathbf{C}_n^b$ = Coordinate transform from navigation/world frame to ADCP/body frame (2σ)
- $\mathbf{v}_v^n$ = Vehicle velocity in the world/navigation frame
- $\mathbf{W}_j$ = Weighting function for each water current velocity from current bin j
- $\mathbf{v}_{c,j}^n$ = water current velocity from current bin j. Each depth cell contains a current velocity state in the X and Y direction, which represents the average velocity of the current through that layer
- $\mathbf{b}_{c,i}$ = Bias in the ith measurement cell in the body frame
- ν_{adcp} = Random noise in the ADCP measurement, given by the sensor manufacturer

Sources of ADCP biases [4] [1] include measurement cell dependent biases, due to beam and sensor misalignment, beam geometry and signal/noise ratio. Sources of ADCP biases due to changing depth include temperature, pressure, scatterers and sound speed estimate error.

These ADCP biases are estimated as the summed effect on the measurement cell observation in the body frame. New bias states are initiated, along with any correlation to the previous bias state in time according to a process model. In order to improve the observability of the ADCP sensor relative biases ($\mathbf{b}_{c,i}$) and allow disambiguation from the true currents ($\mathbf{v}_{c,j}^n$), rotation about heading is required, due to the transformation $\mathbf{C}_n^b$ in Equation 12.

The bias correlation can be modeled as a first order Markov process model of the form

$$\dot{\mathbf{b}}_{c,i} = -\frac{1}{\tau}\mathbf{b}_{c,i} + \nu_{bias} \tag{13}$$

where τ is a time constant which affects the rate at which the bias changes, and ν_{bias} is a random variable with standard deviation [2]

$$\sigma_{bias} = \sqrt{\frac{2f\sigma_{bias\,drift}^2}{\tau}} \tag{14}$$

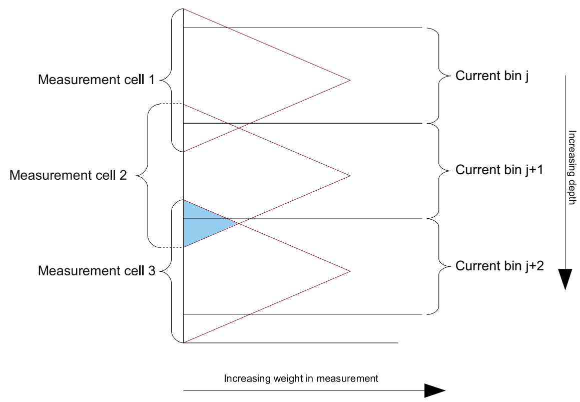

Fig. 2. Depth cell weight functions: depth cells are more sensitive to currents at the center of the cell than at the edges. The area in blue is approximately 15% of the total area of one measurement cell triangle. [4]

where $\sigma_{bias\,drift}$ is the standard deviation of the bias in the long term, a limit to the magnitude of the bias with time, and f is the frequency at which the process model operates. τ is a tuned parameter, which would be determined through accounting for the expected bias drift rate, which may depend and change on a number of factors as described previously. In a discrete form appropriate to be used in the information filter, the observation equation which links the previous bias state to the present bias state is

$$\begin{aligned} \mathbf{z}_{bias\,model} &= \mathbf{b}_{c,i}(t_k) - (1 - \frac{\Delta t}{\tau})\mathbf{b}_{c,i}(t_{k-1}) + \nu_{bias}\Delta t \\ &= 0 \end{aligned} \tag{15}$$

where $\mathbf{b}_{c,i}(t_k)$ is the present bias state, $\mathbf{b}_{c,i}(t_{k-1})$ is the previous bias state, Δt is the time between new bias states $(= 1/f)$.

The ADCP sensor also measures velocities in depth cells with a triangular weight function in the case of the RDI, with 15% overlap with adjacent depth cells as described in the RDI ADCP primer [4], shown in Figure 2. This is due to currents at the centre of the depth cell contributing more to the current bin value than those at the edge of the current bin. Between 2 and 3 depth cells affect each measurement, depending on the depth where the measurement was taken. The weighting for each depth cell depends on the area of the triangle of the measurement cell in that depth cell, and affects Equation 12 with the $\mathbf{W}_j$ term.

III. Results

The results presented in this section to validate the proposed method include a simplified two degree of freedom simulation, a six degree of freedom simulation, and implemention on real data from the ABE AUV.

A. Two degrees of freedom simulation results

The example illustrated in Section II-C and Figures 1(a) to 1(c) can be simulated to examine how the errors evolve in the states. A 1-dimensional current field is simulated in which the vehicle is travelling vertically down, and free to move left or right (but not into and out of the page of the figures). The vehicle experiences unmodelled drag which which causes it move with the currents. The vehicle is also assumed not to pitch in this simulation, resulting in 2 degrees of freedom (2DOF) in translation. To further simplify the analysis of this example, the bias states are not simulated. Table I lists parameter values used for the 2DOF simulation.

TABLE I
Parameter values used in the 2DOF simulation

GPS receiver	Lassen iQ GPS receiver
Initial GPS position fix accuracy	10 m (2σ)
Initial GPS velocity accuracy	0.04 m/s (2σ)
AUV descent rate	0.2 m/s
ADCP make and model	RDI 1200 kHz
ADCP random noise	0.005 m/s (1σ)
ADCP range	30 m
Current bin size	1 m
Simulation time	1000 seconds
Simulated depth	240 m
DVL accuracy	0.006 m/s (2σ)
DVL range	40 m
DVL acquisition time	1000 seconds
ADCP and DVL update rate	5 Hz
Maximum currents	20 cm/s

Figures 3(a) and 3(c) show the position estimate with a constant velocity (CV) model and ADCP aiding respectively before DVL bottom lock. The CV model assumes currents are approximately 20 cm/s at maximum, and no sensor information other than depth observations are available. The position error growth for the CV model is approximately 150m (2σ) over the 1000 second dive, while the ADCP aiding filter position error growth is approximately 40m (2σ).

Figures 4(a) and 4(c) show the velocity estimates for the entire state history for the CV model and ADCP aiding filter respectively before DVL bottom lock. The CV model velocity uncertainty deteriorates to the 20 cm/s water current uncertainty. For ADCP aiding filter, the velocity uncertainty slightly increases with time due to information loss from a finite number of uncertain measurements from the ADCP during the descent. This increase is negligible due to the number of reobservations of the current velocity bins (750 times at most in this case). The error in velocity is primarily from the initial GPS velocity error, at 0.04m/s (2σ).

Figures 3(b) and 3(d) show the position estimate for the entire state history with a CV model and ADCP aiding respectively after DVL bottom lock. The DVL bottom lock constrains some of the velocity history of the dive for the CV model. The position error growth for the CV model is now approximately 90m (2σ) over the 1000 second dive. The DVL bottom lock in the case of the ADCP aiding filter allows the entire velocity history to be constrained due to the correlations of vehicle velocity with water current velocity states. The observation of DVL body-relative velocity is back-propagated to the entire descent because these correlations are properly accounted for. The ADCP aiding filter position error growth is now approximately 6m (2σ).

Figures 4(b) and 4(d) show the velocity estimates for the entire state history for the CV model and ADCP aiding filter respectively after DVL bottom lock. The CV model velocity

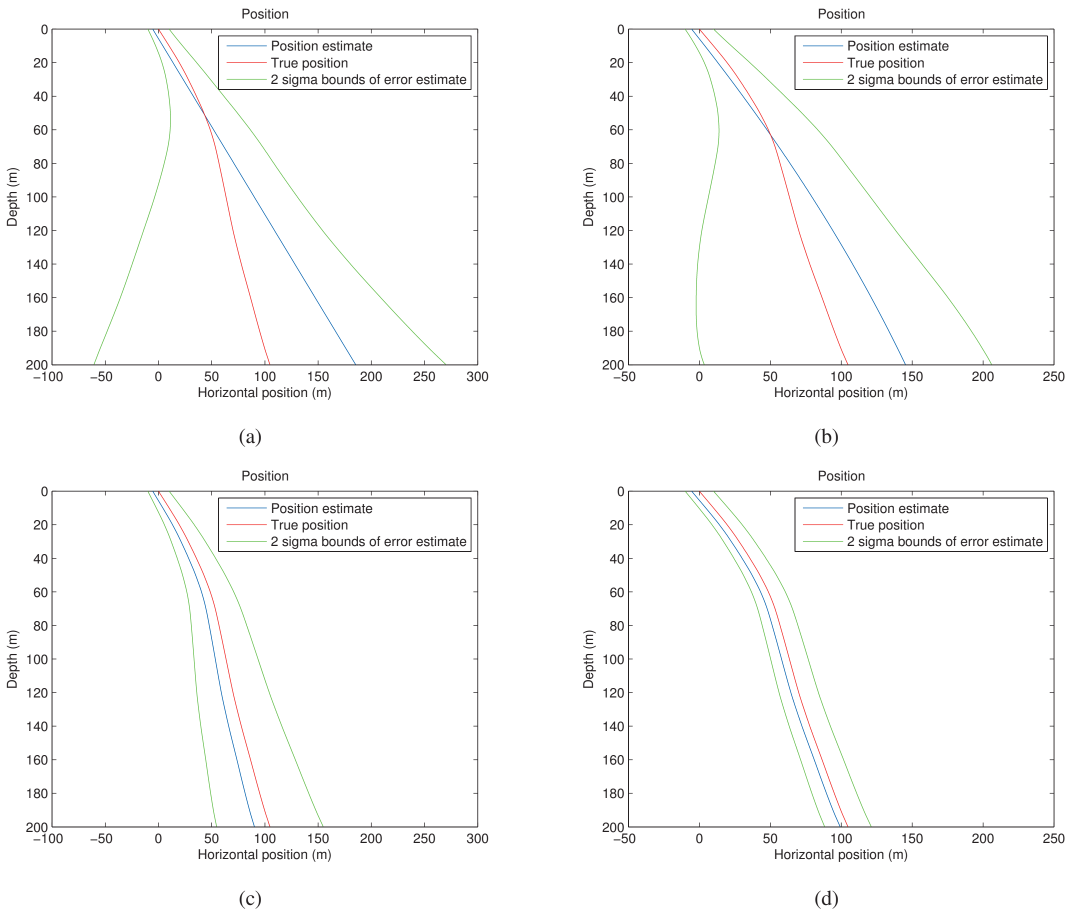

Fig. 3. 2DOF simulation position estimates for the entire state history for the constant velocity model (a) before DVL bottom lock and (b) after DVL bottom lock, and ADCP aiding filter (c) before DVL bottom lock and (d) after DVL bottom lock.

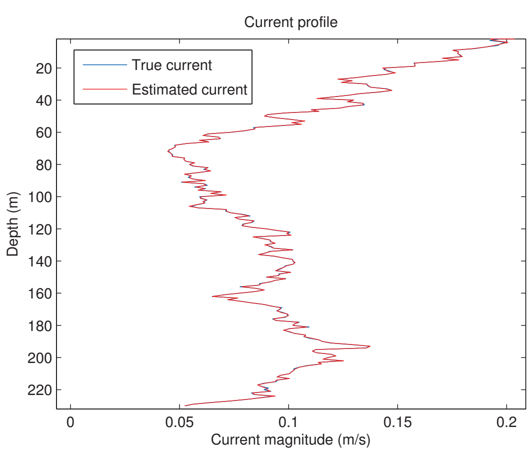

Fig. 5. Current profile derived from the 2DOF simulation

estimates are improved in the time near DVL bottom lock. For the ADCP aiding filter, the entire velocity history estimate error is just above 0.006 m/s (2σ), which is similar to the DVL accuracy, but for the entire dive. It is slightly higher due to the small information loss due to a finite number of uncertain measurements from the ADCP during the descent.

B. Six degrees of freedom simulation results

A six degree of freedom (6DOF) simulation of a typical AUV dive was also completed with the following characteristics: :

1) An initialisation stage to resolve heading using the IMU/GPS.
2) A vertical dive phase, where no GPS or DVL bottom lock is possible. The AUV slowly rotates, and allows sensor biases to be estimated.
3) After 1000 seconds, the vehicle reaches within 40m of the seafloor, and acquires bottom lock to resolve relative velocity.
4) The water current velocities are correlated with depth, with a maximum current around 15 cm/s. This is indicative of a typical current profile [17].

TABLE II
PARAMETER VALUES USED IN THE 6DOF SIMULATION WHICH ARE IN ADDITION OR DIFFERENT TO THE 2DOF SIMULATION

IMU	Honeywell HG1700A58
IMU bias stability	1 degree/hour
AUV rotation rate	3 degrees/second
Maximum currents	15 cm/s
Bias magnitude ($\sigma_{bias\,drift}$)	0.01 m/s (2σ)
Time constant of bias change (τ)	500 seconds

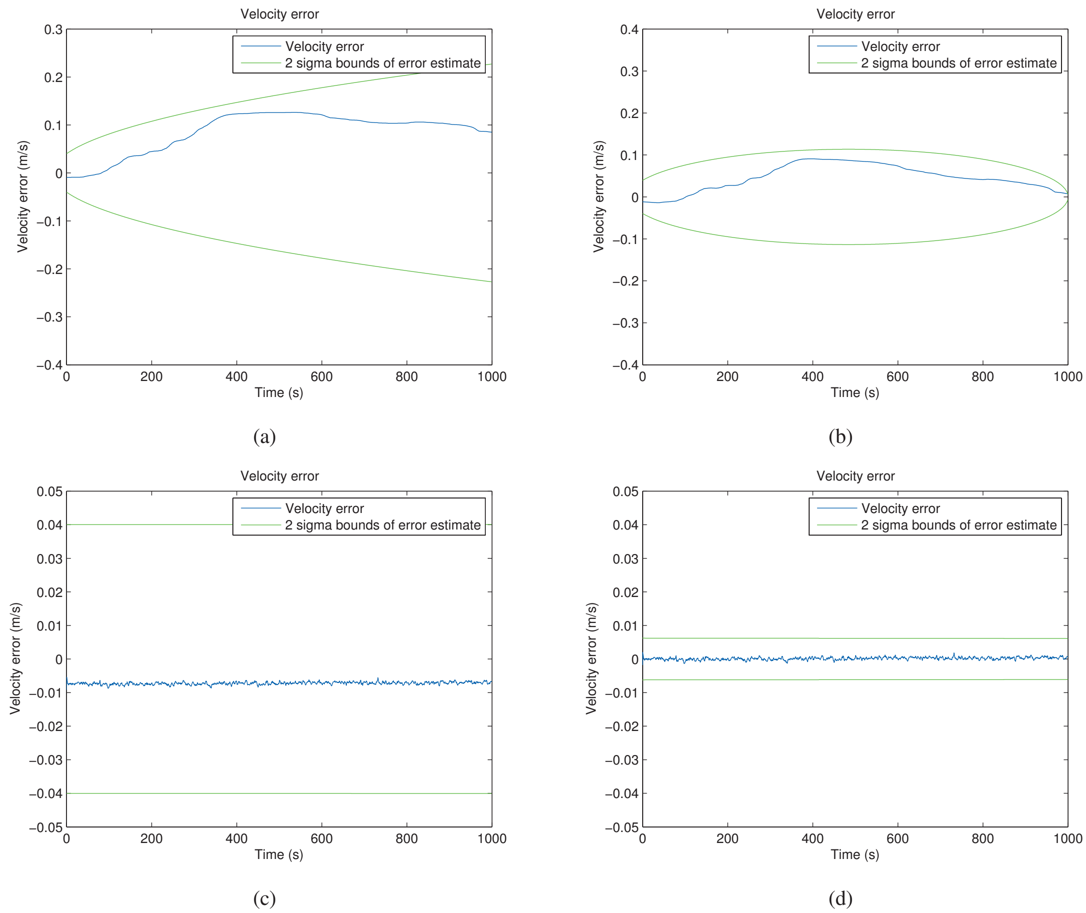

Fig. 4. 2DOF simulation velocity estimates for the entire state history for the constant velocity model (a) before DVL bottom lock and (b) after DVL bottom lock, and ADCP aiding filter (c) before DVL bottom lock and (d) after DVL bottom lock.

Table II summarises the parameter values used in the 6DOF simulation which are in addition or different to the 2DOF simulation. In the subsequent simulation, the measurement cell bias magnitudes are constrained to zero within 0.01 m/s (2σ), in alignment with the RDI specification [4] and the calibration report on the RDI ADCP [13], which contains biases of around 0.01 m/s total at most. The biases change with time in a correlated fashion (which accounts for changing depth during descent), simulating the bias effects described in section II-C2. A value for τ in equation 13 of 500 seconds is used to simulate drifting biases over this time scale.

A Honeywell HG1700A58 IMU was simulated, providing position, velocity and attitude constraints. The method used to incorporate the inertial measurements into the filter are similar to [8], but a global reference frame is used, initial attitude is assumed accurate for linearisation purposes, and an addition to account for Earth rotation (15 degrees/hour is significant in this case) as calculated in [15]:

$$\Delta\phi_{t+1} = \Delta\phi_t + E_t^{t1}(\omega_t^b - bias_w^{obs} - C_n^k\Omega_e^n)\Delta t \qquad (16)$$

where $-C_n^k\Omega_e^n$ is the apparent Earth rotation in the body frame.

As can be seen in Figure 6, the forward (present) filter uncertainty estimate of velocity is constrained to about 0.022 m/s (2σ) in the North and East directions. This uncertainty in velocity during the dive phase is from the initial velocity uncertainty after GPS/INS initialisation/estimation on the surface, with 0.032 m/s error (2σ), which is improved as the velocity constraints allow a better estimate of the previous surface velocity. Given a better initial velocity estimate, the error in velocity will be further reduced during the dive. The velocity uncertainty is also not deteriorating noticeably within the 1000 second time, as there are a large number (at most 750 in this case) of reobservations of the water current bins. Since the water current bins are continually reobserved, the primary source of error in their estimate is from the initial velocity uncertainty.

Referring to Figure 7, after 1000 seconds, just prior to DVL bottom lock, the position error is 22 m (2σ) in the North and East directions.

Figures 8(a) and 8(b) shows the North and East velocity state history for the entire dive after DVL bottom lock. The fluctuation of the velocity uncertainty is heading dependent, as the intial velocity uncertainty on the sea surface is ellipsoidal rather than circular. This results in different amounts of information being stored in different directions in the current profile and bias estimates, and giving different uncertainty depending on orientation. Due to the back-propogation of the DVL body-relative velocity after bottom lock, the velocity uncertainty is

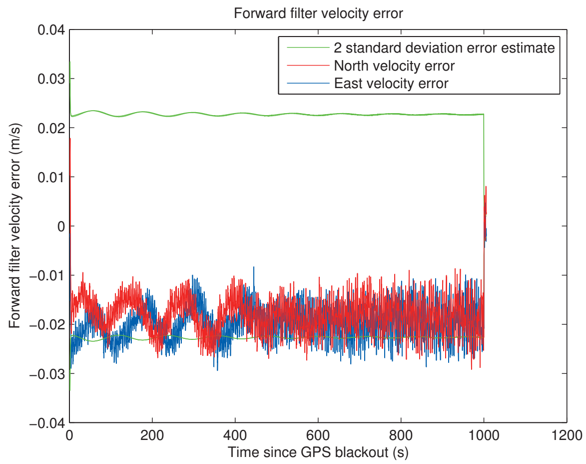

Fig. 6. In the 6DOF simulation, the filter vehicle velocity error is approximately constant as the reobservation of the current bins allows the error to be maintained at below the initial GPS velocity error. Once DVL bottom lock occurs, the velocity uncertainty at that time decreases

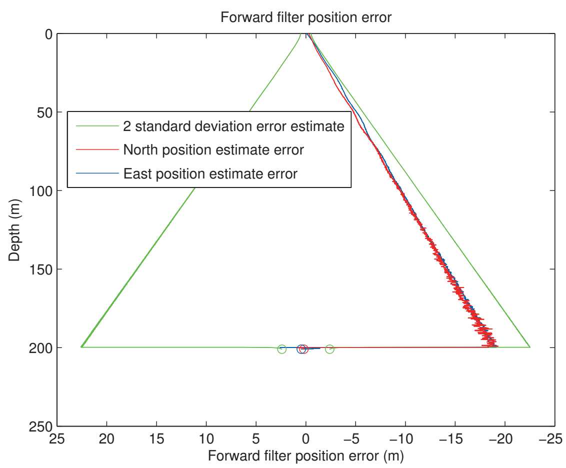

Fig. 7. In the 6DOF simulation, filter vehicle position error grows linearly given the velocity estimates have constant error. Following DVL lock, the error reduces markedly.

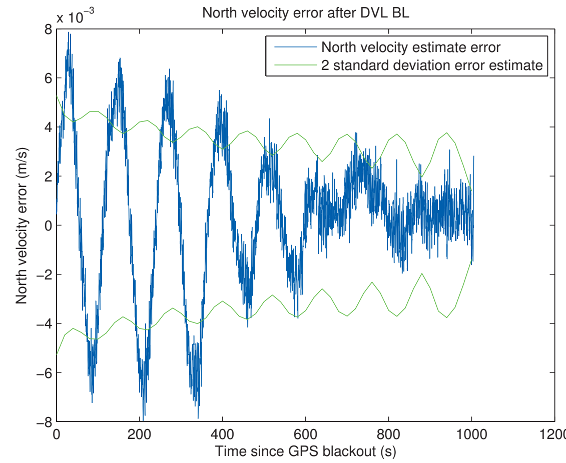

(a)

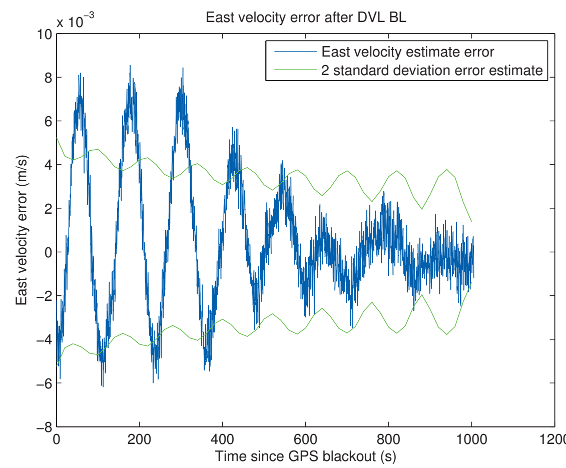

(b)

Fig. 8. Vehicle velocity state history in the (a) North and (b) East directions.

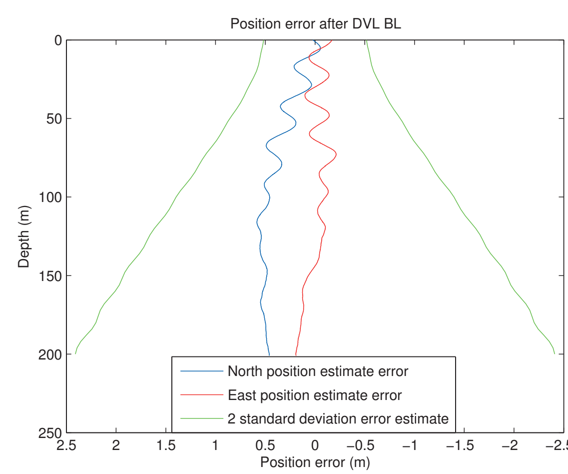

Fig. 9. Position full state history after DVL bottom lock

on average about 3.2 mm/s (20 cm/min) (2σ). This is better than the DVL velocity estimate alone (6 mm/s 2σ) as there is also a low cost IMU providing observations.

Figure 9 show the North and East position error for the entire state history after bottom lock, with a final uncertainty of 2.4 m (2σ) after 1000 seconds.

Figure 10 shows the heading estimate error history from the IMU aided with the ADCP measurements after DVL bottom lock. Initially, the ADCP measurements improves the heading estimate from 0.14 degrees to 0.13 degrees (2σ), as the ADCP measurements give velocity constraints which aid the heading estimate. Later stages show the accumulated error from integrating gyro measurements for the heading increasing the error to 0.22 degrees (2σ).

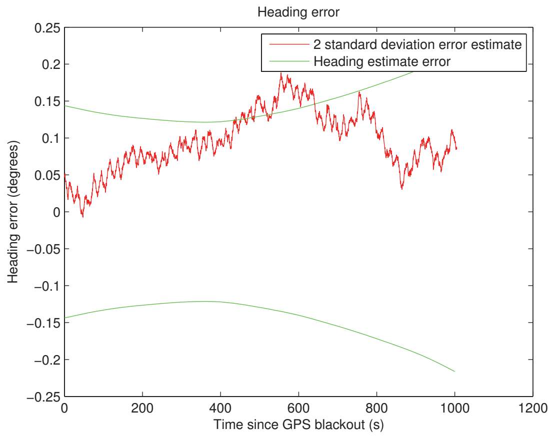

Fig. 10. Heading estimates for the full state history

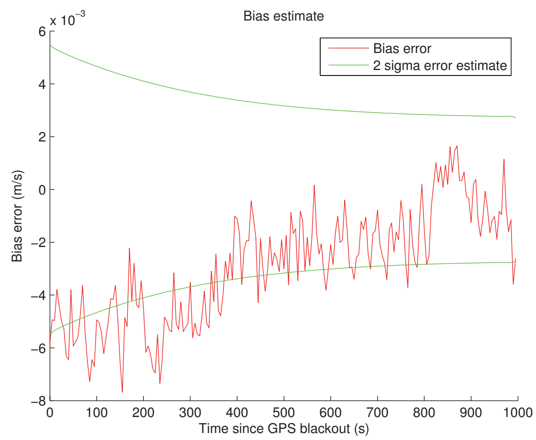

Fig. 11. 10^{th} measurement cell bias error history after DVL bottom lock.

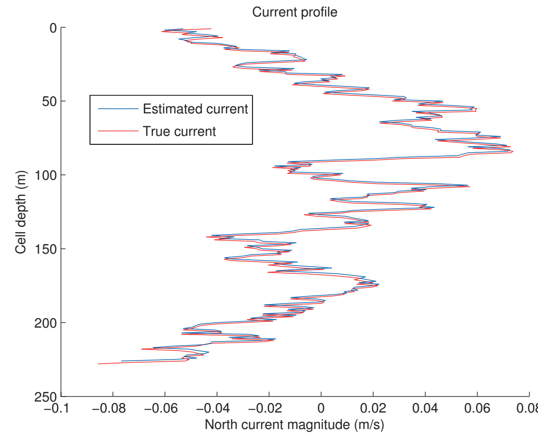

(a)

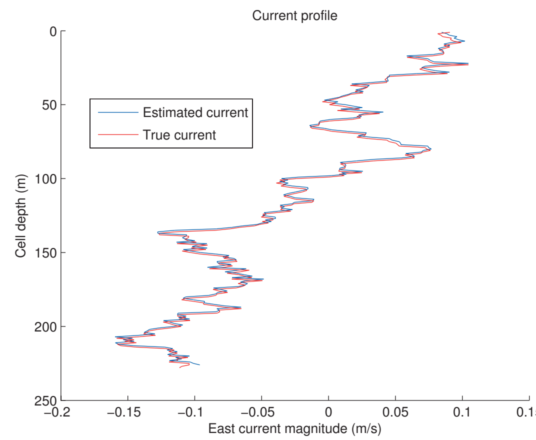

(b)

Fig. 12. Current profile estimate and truth from simulation in the (a) North and (b) East directions

Figure 11 illustrates the 10^{th} measurement cell bias error with time after DVL bottom lock. The bias uncertainty estimate is improved near the DVL bottom lock acquisition.

Figure 12 shows the simulated current, and the estimated current with this filter following DVL bottom lock.

C. Experimental results

Data from an ABE dive on the Southern Mid-Atlantic Ridge [19] was used to evaluate the performance of the ADCP aiding method with real data. A section of data was selected that included LBL observations. The vehicle descent until just before DVL bottom lock was used to drive the filter. Position estimates are compared against the LBL solution (which was not used by the filter). The ADCP aiding method was applied for 1.4 km of dive over a period of 3000 seconds. A compass is available as a heading reference, as an IMU is unavailable on this vehicle. The ADCP used was 300kHz resulting in lower accuracy but longer ranges (up to 100m) compared to the simulation ADCP which was a 1200kHz model. ADCP observations are received at 2Hz with measurement cells (and therefore current bins) 10m in size.

Error gating is achieved by noting that consecutive readings from the same bins should not vary substantially from the predicted reading by more than the sensor uncertainty permits and predicted water current velocity changes.

The ABE vehicle rotates as it descends, so biases can be distinguished. Further work needs to be made to characterise the bias behaviour and modelling, in this case the behaviour of τ in Equation 13. A value for τ of 500 seconds gave good performance, and results use this value.

Initial velocity is derived by using the LBL and ADCP measurements combined. The initial velocity accuracy is 2.6 cm/s (2σ) according to the filter.

It should be noted that just prior to achieving bottom lock, the ADCP data is corrupted so there is no data to link between ADCP aiding and the DVL bottom lock. As a result, the DVL velocity constraint has not back propogated to decrease the errors, as in the simulation. The DVL bottom finding pings are the likely cause as they interfere with the ADCP readings if not configured correctly. As evidenced by Visbeck's results in [17], possible solutions do exist. Addressing this issue remains as future work.

The ADCP derived position matches well with the LBL

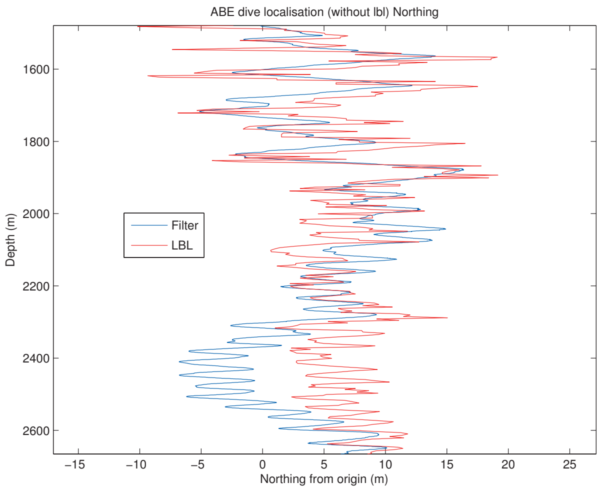

(a)

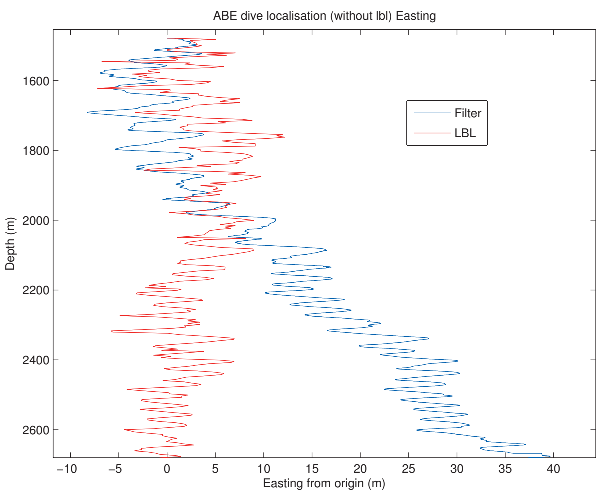

(b)

Fig. 13. Vehicle position estimates in the (a) North and (b) East direction. The initial velocity accuracy of 2.6 cm/s (2σ) results in an approximately 78 metres (2σ) standard deviation in position error after about 3000 seconds

positioning as seen in Figure 13, with drift observable in the East direction of about 39 metres due to accumulated velocity error. The position uncertainty estimate from the filter is 78 metres (2σ) after 3000 seconds. Variations in the bias estimates can be observed with depth change over time in Figure 14, indicating a depth dependance. Figure 15 shows the estimated current profile, illustrating the variable nature of the observed currents with depth.

D. Application of ADCP aiding method to whole ABE dive

The ABE mission where this data is used from is for hydrothermal vent localisation [6]. The required accuracy to achieve the nested survey strategy of homing in on the hydrothermal vent location is in the order of tens of metres, requiring the LBL localisation method to be utilised.

By extrapolating the results of the simulation to this mission, if the ADCP method is applied for the entire dive from surface GPS, prior to DVL bottom lock the position error growth will

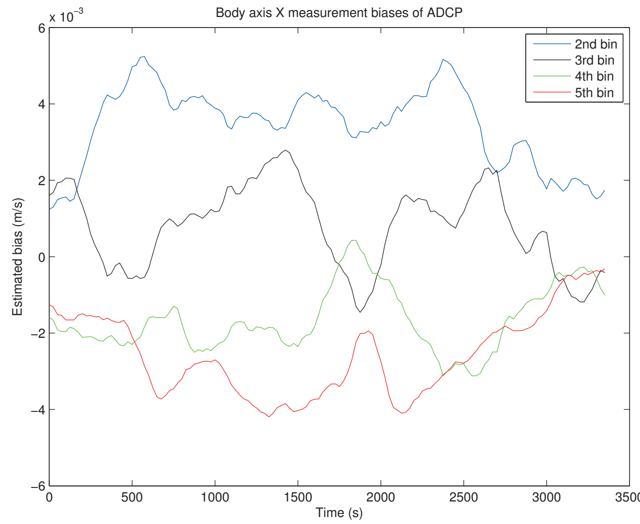

(a)

(b)

Fig. 14. Body relative measurement cell biases from the ABE dive in the (a) forward and (a) starboard directions. Bias estimates are observed to change with time, due to changing pressure, temperature and biology, and are differing in magntitude depending on measurement bin.

be about 320m (2σ) after 8000 seconds of the full 3 km dive. Once DVL bottom lock is acquired, the position error growth will be about 48m (2σ). This is still not able to compete with the accuracy of the acoustic LBL method. With the addition of a low cost IMU, position error growth is about 176m (2σ) before DVL bottom lock, and about 25m (2σ) is possible after DVL bottom lock. This is approaching the perfomance the LBL method for the ABE mission.

The error growth in position before bottom lock is dependent on the intial velocity uncertainty. According to van Graas [16], 4-8 mm/s velocity error (2σ) in the horizontal directions is possible with standard GPS by using carrier phase GPS velocity. This is in constrast to the 4 cm/s (2σ) GPS velocity error used in simulations for the Lassen iQ. This means that initial velocity error and thus descent position error growth can also be constrained to the 4-8 mm/s (2σ) range,

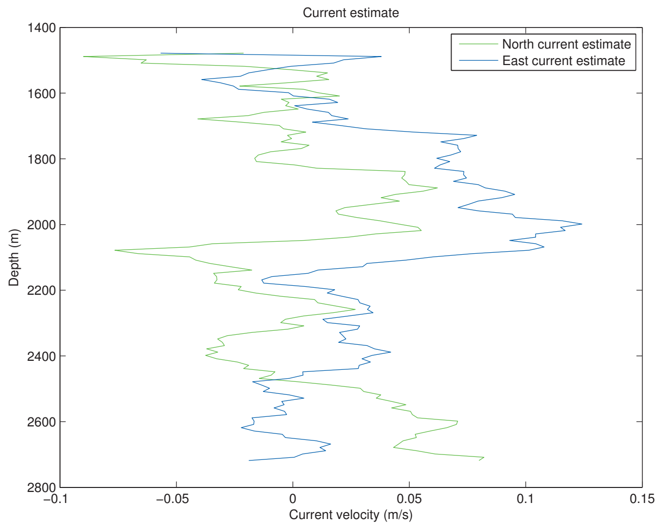

Fig. 15. The estimated current profile using the filter, illustrating the scale of changes in currents over 1.4 km of dive

which is similar to DVL velocity uncertainty. This results in around 20m (2σ) position error growth prior to DVL bottom lock with a low cost IMU, and allowing even better localisation once bottom lock is achieved. Thus, the ADCP aiding method is a viable alternative to LBL in this case. Further work will incorporate carrier phase GPS velocity modelling.

IV. Conclusion

By utilising this method to incorporate ADCP measurements, transitting between the sea-surface and the sea-floor will have constrained error growth in position and velocity. This makes it appropriate for long term, accurate navigation of an AUV which dives and resurfaces, and requires underwater position accuracy close to the seafloor. The result is a solution which allows accurately positioned autonomous diving in situations where bottom lock is not available through the dive.

Further work will incorporate the sea floor portion of the dive (DVL and SLAM), along with ascent from the sea floor to the sea surface (ADCP) into a full non-linear optimisation of the entire mission, resulting in a fully georeferenced survey mission without the need for external acoustic localisation.

Also, work must be done to analyse the ADCP bias behaviour and arrive at conclusions regarding the correct method to model these biases, although preliminary steps have been taken in this paper.

Accounting for prior information about water currents will also aid the localisation. Accommodating horizontally looking ADCPs and spatiotemporal water current evolution models, along with more generalised methods to discretise the state space (into 3D current voxels) will further generalise this method to other situations beyond vertical dives.

To further validate this method on real AUV missions, data is to be collected where the DVL configuration does not interfere with the ADCP measurements as in the ABE mission. Also, an IMU can be incorporated to show the performance improvement on real data that is observed in simulation.

Implications for path planning and the incorporation of a vehicle model within the mapped water current environment are also yet to be explored.

Acknowledgment

This work is supported by the ARC Centre of Excellence programme, funded by the Australian Research Council (ARC) and the New South Wales State Government. The authors would also like to thank the Woods Hole Oceanographic Institution for making data from ABE trials available to validate this work.

References

[1] C. Atkinson. Analysis of shipboard ADCP data from RRS Discovery Cruise D324: RAPID Array Eastern Boundary. 2008.

[2] W.S. Flenniken IV. Modeling inertial measurement units and analyzing the effect of their errors in navigation applications. *Auburn University Masters Thesis*, 2005.

[3] B. Garau, A. Alvarez, and G. Oliver. AUV navigation through turbulent ocean environments supported by onboard H-ADCP. In *Robotics and Automation, 2006. ICRA 2006. Proceedings 2006 IEEE International Conference on*, pages 3556–3561, 2006.

[4] R.L. Gordon and RD Instruments. Principles of Operation a Practical Primer. *RD Instruments, San Diego*, 1996.

[5] O. Hegrenaes and E. Berglund. Doppler water-track aided inertial navigation for autonomous underwater vehicle. In *OCEANS 2009-EUROPE, 2009. OCEANS '09.*, pages 1–10, May 2009.

[6] M.V. Jakuba. *Stochastic mapping for chemical plume source localization with application to autonomous hydrothermal vent discovery*. PhD thesis, Massachusetts Institute of Technology and Woods Hole Oceanographic Institution, 2007.

[7] J.C. Kinsey, R.M. Eustice, and L.L. Whitcomb. A survey of underwater vehicle navigation: Recent advances and new challenges. In *Proceedings of the 7th Conference on Maneuvering and Control of Marine Craft (MCMC2006). IFAC, Lisbon*. Citeseer, 2006.

[8] T. Lupton and S. Sukkarieh. Efficient integration of inertial observations into visual slam without initialization. In *Intelligent Robots and Systems, 2009. IROS 2009. IEEE/RSJ International Conference on*, pages 1547–1552, Oct. 2009.

[9] M. Mandt, K. Gade, and B. Jalving. Integrating DGPS-USBL position measurements with inertial navigation in the HUGIN 3000 AUV. In *Proceedings of the 8th Saint Petersburg International Conference on Integrated Navigation Systems, Saint Petersburg, Russia*, 2001.

[10] R. McEwen, H. Thomas, D. Weber, and F. Psota. Performance of an AUV navigation system at Arctic latitudes. *IEEE Journal of Oceanic Engineering*, 30(2):443–454, 2005.

[11] F. Napolitano, A. Chapelon, A. Urgell, and Y. Paturel. PHINS: The autonomous navigation solution. *Sea Technology*, 45(2):55–58, 2004.

[12] P.E. Plimpton, H.P. Freitag, and M.J. McPhaden. ADCP Velocity Errors from Pelagic Fish Schooling around Equatorial Moorings*. *Journal of Atmospheric and Oceanic Technology*, 14(5):1212–1223, 1997.

[13] H.H. Shih, C. Payton, J. Sprenke, and T. Mero. Towing basin speed calibration of acoustic Doppler current profiling instruments. In *Proc. 2000 Joint Conference on Water Resources Engineering and Water Resources Planning and Management*.

[14] S. Thrun, Y. Liu, D. Koller, A.Y. Ng, Z. Ghahramani, and H. Durrant-Whyte. Simultaneous localization and mapping with sparse extended information filters. *The International Journal of Robotics Research*, 23(7-8):693, 2004.

[15] D.H. Titterton and J.L. Weston. *Strapdown inertial navigation technology*. Peter Peregrinus Ltd, 2004.

[16] F. van Graas and A. Soloviev. Precise velocity estimation using a stand-alone GPS receiver. *Navigation(Washington, DC)*, 51(4):283–292, 2004.

[17] M. Visbeck. Deep velocity profiling using lowered acoustic Doppler current profilers: Bottom track and inverse solutions. *Journal of Atmospheric and Oceanic Technology*, 19(5):794–807, 2002.

[18] S.B. Williams, O. Pizarro, I. Mahon, and M. Johnson-Roberson. Simultaneous Localisation and Mapping and Dense Stereoscopic Seafloor Reconstruction Using an AUV. *in G. Pappas, V. Kumar and O. Khatib, Springer Tracts in Advanced Robotics*, 54.

[19] D.R. Yoerger, M. Jakuba, A.M. Bradley, and B. Bingham. Techniques for deep sea near bottom survey using an autonomous underwater vehicle. *International Journal of Robotics Research*, 26(1):41–54, 2007.